A&A 403, 141–154 (2003)
DOI: 10.1051/0004-6361:20030208

Astronomy & Astrophysics

Stellar sources in the ISOGAL intermediate bulge fields⋆,⋆⋆,⋆⋆⋆

D. K. Ojha[1], A. Omont[2], F. Schuller[2], G. Simon[3], S. Ganesh[4], and M. Schultheis[2]

[1] Tata Institute of Fundamental Research, Homi Bhabha Road, Colaba, Mumbai 400 005, India
[2] Institut d'Astrophysique de Paris, CNRS, 98bis Bld. Arago, 75014 Paris, France
e-mail: omont@iap.fr
[3] GEPI, Observatoire de Paris, 61 Av. de l'Observatoire, 75014, Paris, France
[4] Physical Research Laboratory, Navarangpura, Ahmedabad 380009, India

Received 3 June 2002 / Accepted 11 February 2003

Abstract. We present a study of ISOGAL sources in the "intermediate" galactic bulge ($|l| < 2°$, $|b| \sim 1°$–$4°$), observed by ISOCAM at 7 and 15 μm. In combination with near-infrared (I, J, K_s) data of DENIS survey, complemented by 2MASS data, we discuss the nature of the ISOGAL sources, their luminosities, the interstellar extinction and the mass-loss rates. A large fraction of the 1464 detected sources at 15 μm are AGB stars above the RGB tip, a number of them show an excess in $([7]–[15])_0$ and $(K_s–[15])_0$ colours, characteristic of mass-loss. The latter, especially $(K_s–[15])_0$, provide estimates of the mass-loss rates and show their distribution in the range 10^{-8} to 10^{-5} $M_\odot$ yr^{-1}.

Key words. stars: AGB and post-AGB – stars: circumstellar matter – stars: mass-loss – dust: extinction – infrared: stars – Galaxy: bulge

1. Introduction

ISOGAL is a detailed mid-infrared imaging survey of the inner galaxy, tracing the galactic structure and stellar populations (Omont et al. 2003). It combines 7 and 15 μm ISOCAM data with IJK_s DENIS data (Epchtein et al. 1994, 1997; Simon et al., in preparation). The main goals of ISOGAL survey are to trace the large scale inner disk and bulge structure using primarily red giants old stars; to study the corresponding stellar populations; to trace the age and mass-loss of AGB stars; to determine the number of (dusty) young stars and to map the star formation regions through diffuse ISM emission and extinction. Multicolour near- and mid-infrared data are essential to analyse these features.

The scientific results of ISOGAL are summarized in Omont et al. (2003). The analysis of the first ISOGAL field is detailed in Pérault et al. (1996). The discussion of a small field in the inner bulge ($\ell = 0°$, $b = +1°$) (Omont et al. 1999) has confirmed and characterized the remarkable capability of ISOGAL to detect the mass-losing AGB stars. Glass et al. (1999) analysed the ISOGAL fields in Baade's Windows of low obscuration towards the bulge. Most of the detected objects towards Baade's Windows are late-type M stars, with a cut-off for those earlier than about M3–M4. In the same fields, Alard et al. (2001) have determined the general properties of a well defined sample of semi-regular variables by obtaining the MACHO lightcurves in V and R for a large fraction (∼300) of the ISOGAL objects in Baade's Windows. Recently, Schultheis & Glass (2001) and Glass & Schultheis (2002) have further investigated the luminous M-type giants in these Baade's Windows fields, in the near-infrared mainly taken from the DENIS and 2MASS (Skrutskie et al. 1995) surveys.

In this paper, we report the study of nine ISOGAL fields in the intermediate galactic bulge ($-1.5° < \ell < +1.6°$; $-3.8° \leq b \leq -1.0°$, $b = +1.0°$ (Fig. 1); with a total area ∼0.29 deg^2) and more than 2300 detected sources. The 15 μm and 7 μm ISOGAL point sources have been combined primarily with DENIS IJK_s data in the ISOGAL–DENIS Point Source Catalogue which gives magnitudes I, J, K_s, [7], [15] (Schuller et al. 2003) – and also with 2MASS (J, H, K_s) and MSX (mid–IR, Price et al. 2001) – to determine their nature and the interstellar extinction. Analysis at five near- and mid-infrared wavelengths of the ISOGAL sources, together with the relatively low and constant extinction, shows that the majority of the sources are red giants with luminosities just above or close to the RGB tip and with a large proportion of detectable mass-loss. The various colour-colour and magnitude-colour

Send offprint requests to: D. K. Ojha, e-mail: ojha@tifr.res.in
⋆ This is paper No. 14 in a refereed journal based on data from the ISOGAL project.
⋆⋆ Based on observations with ISO, an ESA project with instruments funded by ESA Member States (especially the PI countries: France, Germany, The Netherlands and the UK) and with the participation of ISAS and NASA.
⋆⋆⋆ Based on observations collected at the European Southern Observatory, La Silla, Chile.

diagrams are discussed in the paper, together with values of the luminosities and mass-loss rates.

The outline of the paper is as follows: In Sect. 2, we present the ISOGAL and DENIS observations, as well as complementary 2MASS (and MSX) data. Section 3 describes the cross-identification of the mid-IR ISOGAL sources between 7 and 15 μm bands and then with near-infrared sources. In Sect. 4, we discuss the determination of interstellar extinction in the line of sight of the bulge fields using the isochrone fitting. Section 5 presents the derivation of bolometric magnitude ($M_{\rm bol}$) and luminosity for each star in the bulge fields. In Sect. 6, we discuss the nature of ISOGAL sources. Section 7 is devoted to the derivation of mass-loss rates based on $(K_{\rm s}$–$[15])_0$ colour. In Sect. 8, we consider a preliminary estimation of the total mass-loss rate in the intermediate bulge.

2. ISOGAL observations and complementary data

ISOGAL observations with ISOCAM (see Césarsky et al. 1996 for a general reference to ISOCAM operation and performances) at 6″ pixel field of view of nine intermediate bulge fields with good quality of 7 and 15 μm data are used in our study (see Fig. 1). These observations were performed during 1996–1998 at 15 μm (filter LW3: 12–18 μm or LW9: 14–16 μm), and at 7 μm (filter LW2: 5.5–8.5 μm or LW6: 7.0–8.5 μm) (Table 1). For all the observed ISOGAL fields, we have used the data of the ISOGAL Point Source Catalogue (PSC, version 1) described in Schuller et al. (2003), reproduced, for our nine fields, in a shortened version in Table 2 available at CDS[1]. They were derived with an improved data reduction with respect to ISO Archive data, with the use of CIA ISOCAM software and of a special source extraction (Schuller et al. 2003). From the comparison between the different observations of the field at $l = 0°$, $b = +1°$, we find very small differences between the different filters: LW2–LW6 = +0.05 mag & LW3–LW9 = +0.1 mag. Hence, no corrections are applied in LW6 and LW9 magnitudes to jointly discuss them with the main LW2 and LW3 data. The total number of sources in the nine fields are 2232 and 1464 at 7 and 15 μm, respectively, with a grand total of 2354 sources. The corresponding average source densities are $\sim 8 \times 10^3$ deg^{-2} and $\sim 5 \times 10^3$ deg^{-2} at 7 and 15 μm, respectively (see detailed density for each field as shown in Table 1). The 7 and 15 μm magnitude limits of the ISOGAL PSC are given in Table 1 and vary from 8.6 to 9.5 at 7 μm, and from 7.5 to 8.5 at 15 μm. Generally, these ISO cutoff magnitudes should roughly correspond to a detection completeness level close to ∼50%, and depend on the source density, so that these magnitude limits vary by about 1 mag among the different fields. The histograms of the 7 and 15 μm total source counts derived from the 6″ ISOGAL observations are displayed in Fig. 2. This figure also displays the data (available at IPAC, version 1.2) of the MSX sources detected in these fields (108 at 8 μm, all with $[7]_{\rm ISO} < 7.0$ and 16 at 15 μm, all with $[15])_{\rm ISO} < 4.5$). They show the large difference in sensitivity and in the number of detected sources between the two surveys. We have checked the consistency of ISOGAL and MSX 15 μm magnitudes for the 13 strongest sources (with $[15] < 3.5$, in order to avoid the Malmquist bias). The average difference is $[15]_{\rm ISO}$–$[15]_{\rm MSX} = -0.06 \pm 0.43$, where the large dispersion is probably related to the source variability.

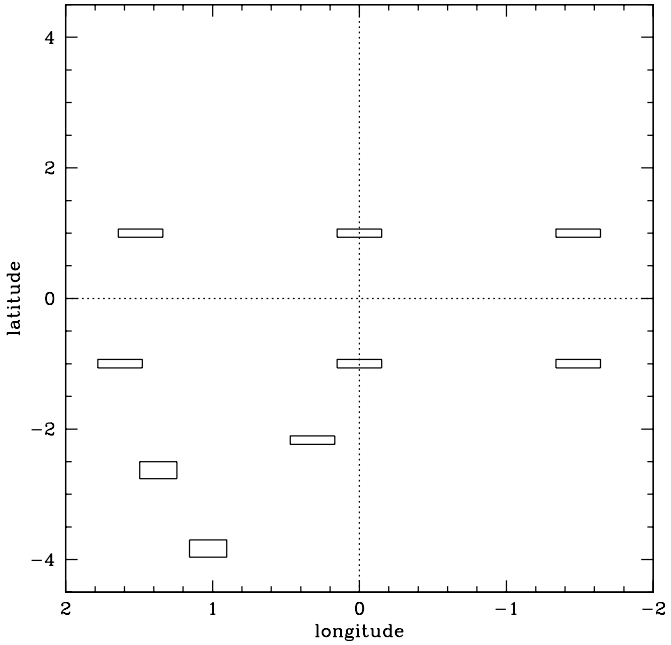

Fig. 1. The rectangles show the limits of the ISOGAL fields studied in this paper.

In the near-infrared, the data mostly used in this paper are also those of the PSC of the ISOGAL–DENIS survey. They are complemented by the 2MASS data (from the Point Source Catalog of the 2MASS second release available at IPAC and CDS). However, these 2MASS data do not fully cover all the nine ISOGAL fields. There are large blank areas (because of saturating stars) in three fields, so that only about 88% of the total area of the nine ISOGAL fields is covered. All sources in these 2MASS data have detections in the three $JHK_{\rm s}$ bands. The DENIS near-infrared data are acquired from the DENIS survey with special observations of the Galactic bulge (Simon et al., in preparation) in the three bands, I (0.80 μm), J (1.25 μm) and $K_{\rm s}$ (2.17 μm), which completely cover the nine considered ISOGAL bulge fields. Therefore, we have taken the more complete DENIS data as the main reference for near-infrared associations.

The histograms of all the DENIS I, J, $K_{\rm s}$ sources in the observed fields are shown in Fig. 3. The completeness limit is close to 12.0 in $K_{\rm s}$ band, 14.0 in J band and 15.5 in I band, respectively. However, only near-infrared sources with $K_{\rm s} \lesssim 11.0$ are used for near-infrared cross-identifications, in order to limit the number of spurious associations (see Sect. 3 and Table 1). Figure 3 also displays the histograms of J, H and $K_{\rm s}$ 2MASS sources. We have compared the DENIS and 2MASS photometry of 1963 stars common in ISOGAL–DENIS PSC and

[1] Table 2 contains the catalogue of ISOGAL-DENIS sources from nine bulge fields with their 2MASS & MSX counterparts. The catalogue will be available at the CDS via anonymous ftp to `cdsarc.u-strasbg.fr (130.79.128.5)` or via `http://cdsweb.u-strabg.fr/cgi-bin/qcat?J/A+A/403/141`.

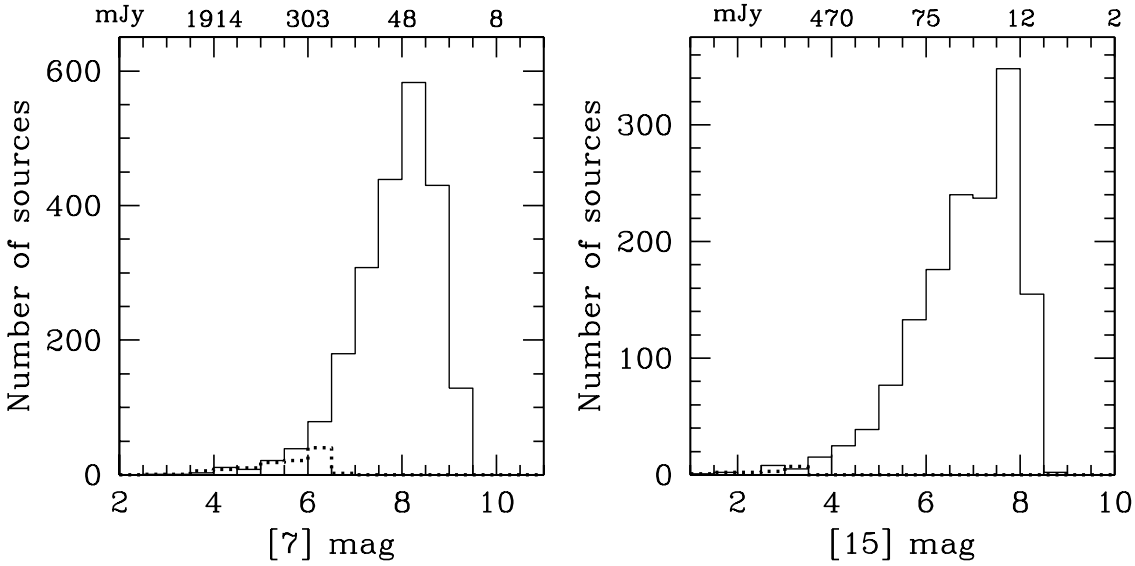

Fig. 2. 7 and 15 μm source distributions in half magnitude bins. ISOGAL magnitudes are converted into flux densities using the relations given in Schuller et al. (2003). The dotted lines show the MSX A (~8 μm) and D (~15 μm) sources cross-identified with ISOGAL 7 and 15 μm sources. MSX magnitudes are derived using the zero magnitude flux given by Egan et al. (1999).

2MASS in our nine fields. We find small differences in the averages: $K_{\rm DENIS}-K_{\rm 2MASS} = -0.00 \pm 0.07$ and $J_{\rm DENIS}-J_{\rm 2MASS} = -0.02 \pm 0.09$; hence no corrections are applied.

Table 1 shows the used ISOGAL, DENIS and 2MASS observations in detail. It should be noted that the majority of the observations were performed on dates with large differences (from two months to three years), except for 7 and 15 μm observations performed on the same date in six fields out of nine, and the DENIS, 2MASS observations performed on the same date for all sources in their respective bands. Such differences in dates are comparable to the period of Long Period Variables (LPVs). One thus expects that the corresponding colours of the few large amplitude and variables (Miras) may be strongly affected. This uncertainty will propagate through to the final uncertainties in luminosity and mass-loss as well. From the detailed studies of LPVs in the two Baade's Window fields (see Glass et al. 1999; Alard et al. 2001; Schultheis & Glass 2001; Glass & Schultheis 2002), one can estimate that the variability rms error in the near-infrared is $\simeq$0.3 mag for strong variables (miras), i.e. most of the strong sources with [15] < 4, and less than 0.1 mag for most others. In order to reduce this uncertainty by about a factor $\sqrt{2}$, we have systematically used: 1) The average of DENIS and 2MASS J and $K_{\rm s}$ magnitudes when available; however, the DENIS sources are saturated at $K_{\rm s} \lesssim 6.5$, and, for such few strong sources, only 2MASS data are used (Sect. 3); 2) The average of ISOGAL and MSX 15 μm magnitudes for the few (13) strong sources detected by MSX with $[15]_{\rm ISO} < 3.5$.

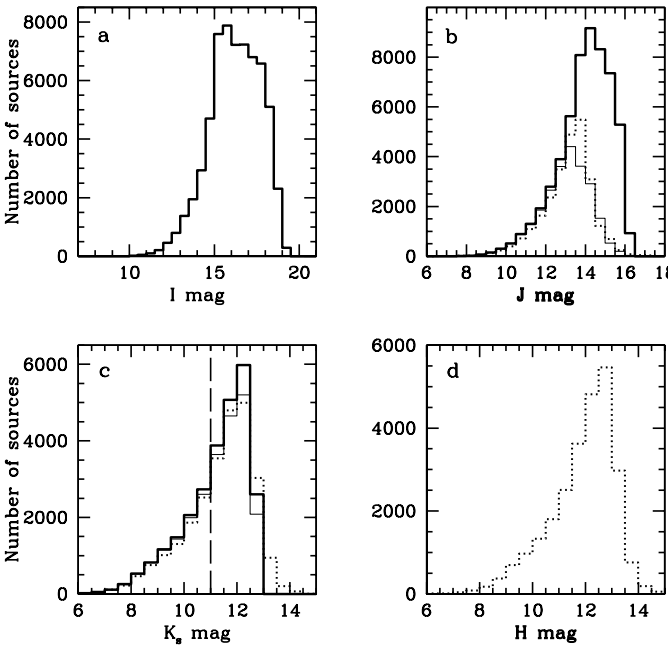

Fig. 3. DENIS source counts in I, J and $K_{\rm s}$ bands in half magnitude bins (thick continuous lines). Thin continuous lines show the DENIS sources detected in J and $K_{\rm s}$ bands. Dotted lines show the 2MASS sources detected in J, H and $K_{\rm s}$ bands. The used 2MASS data (2nd release) contain only sources detected in the three $JHK_{\rm s}$ bands and cover only ~88% of the total area of the considered ISOGAL fields. Long-dashed line shows the average $K_{\rm s}$ magnitude cut of DENIS sources ($K_{\rm s} < 11$, see Table 1 and Sect. 3) cross-identified with ISOGAL sources.

3. Cross-identification of ISOGAL and near-infrared sources

In order to perform the association between 7 and 15 μm sources in the ISOGAL PSC, first a global offset between the two sets of coordinates has been determined, then distortion coefficients have been computed to correct for the rotation effects (Schuller et al. 2003). Finally, 7 and 15 μm associations were searched within a radius of twice the size of the pixel ($2 \times 6'' = 12''$). Only ~8% (122) of the 15 μm sources have no 7 μm counterpart. However, out of these 122 15 μm

Table 1. Log of ISOCAM, DENIS and 2MASS observations in the intermediate bulge fields.

ISOGAL Field	ISOGAL Obs.	Filter	Date of ISOGAL Obs.	Source densities at 7 and 15 μm (per deg^2)	7 and 15 μm mag limits	Date of DENIS IJK_s Obs.	Date of 2MASS JHK_s Obs.	Mean A_V	DENIS K_{sLim}
–01.49–01.00	83801111	LW2	02/03/98	8500	9.03	22/05/99 &	14/08/98	11.8	11.4
	32500342	LW3	06/10/96	5231	8.12	08/07/99			
+00.00–01.00	84100926	LW2	05/03/98	10607	8.80	01/05/99	16/07/98	8.1	10.5
	84100927	LW3	05/03/98	6929	7.93				
+01.63–01.00	84101405	LW6	05/03/98	6538	8.61	03/07/98	16/07/98	6.3	10.9
	84101406	LW9	05/03/98	3654	7.53				
–01.49+01.00	83701309	LW2	01/03/98	9111	8.94	29/08/98	02/07/98	6.0	10.8
	32500238	LW3	06/10/96	6556	8.04				
+00.00+01.00	83600418	LW2	28/02/98	9259	8.89	18/05/98	02/07/98	6.3	10.6
	83600523	LW3	28/02/98	6148	8.00				
+01.49+01.00	84001007	LW6	04/03/98	7962	8.65	09/05/99	02/07/98	6.4	10.9
	32500239	LW3	06/10/96	6077	7.99				
+01.37–02.63	83800913	LW2	02/03/98	6660	9.15	13/09/98 &	16/07/98	1.2	11.4
(Sgr I BW field)	83800914	LW3	02/03/98	4453	8.33	20/06/99			
+01.03–03.83	84001115	LW2	04/03/98	5608	9.48	15/09/98	15/08/98	1.5	12.0
(NGC 7522 BW	84001116	LW3	04/03/98	3333	8.51				
field)									
+00.32–02.17	84100428	LW2	05/03/98	7519	9.14	20/05/98	16/07/98	2.2	11.0
	84100429	LW3	05/03/98	4889	8.26				

sources, a large fraction (77%: 94 sources) have been associated with K_s ($K_s \lesssim 11.0$) DENIS or 2MASS sources, which reflects the incompleteness of weak 7 μm sources. The rms of the [7]–[15] separations has a small value equal to 1.5″, which shows the good quality of most of the associations. Indeed, 98% have a quality factor 3 or 4 in the ISOGAL PSC which warrants almost certainly real association (Schuller et al. 2003), only 2% have a quality factor 2 which means that the association is probably real, but should be considered with some care (a few doubtful associations with quality factor 1 have been discarded).

A cross-correlation algorithm similar to the one used to associate 7 and 15 μm data has been used to look for DENIS counterparts to ISOGAL sources (Schuller et al. 2003). The density of DENIS sources is so high that the DENIS catalogues were cut to 36 000 sources per square degree ($K_s \lesssim 11.0$, see Table 1). A search radius of 7″ was initially used for the cross-correlation between ISOGAL and DENIS sources, and the association was limited to DENIS sources detected in K_s. Figure 4 shows the histogram of positional difference of ISOGAL–DENIS cross-identified sources in our nine fields. The rms of the distances of ISOGAL-DENIS association has a value equal to 1.4″. About 98% of the ISOGAL sources (either 7 or 15 μm) have thus initially an association with a DENIS source with $K_s \lesssim 11.0$. Even with such a large search radius, because the proportion of real associations is very large and only associations with the smallest separation are retained, the fraction of false associations is expected to remain ~1%. In addition, the quality of the associations is characterised by a specific flag and we have dropped in Table 2 the associations with the poorest quality (see below). Such a large radius was indeed needed since, in some cases, real associations have such large separation, because of the large pixels and undersampling of ISOGAL, in particular in the cases of blended or slightly extended sources. This is extensively discussed in Schuller et al. (2003). About 1% of the ISOGAL sources (23) have a DENIS counterpart which are saturated ($K_s \lesssim 6.5$, see Fig. 7), out of which 18 saturated DENIS sources have been replaced by the 2MASS sources (as indicated in Table 2 available at CDS). The five other sources are not identified in the published 2MASS fields. Out of these 18 sources, 50% sources are identified as foreground and taken out of the stars further discussed in the paper (see text, Sect. 4) and the remaining are shown in various figures (see Figs. 8, 9, 11 and 12). Most of the ISOGAL sources cross-identified with DENIS ones (92%) have a good quality association (quality flags 4 and 5; see Schuller et al. 2003 for details), 7% sources have more doubtful association (quality flags 2 and 3) and only less than 1% ones have very bad association (quality flag 1). For the present study, we have dropped in Table 2 the sources which have association quality flag of 1 (15 associations) and those with associated distance of more than 5″ (12 associations, mostly with quality flag 2). The number of contaminating false matches is thus kept well below 1%. The respective numbers of 7 μm alone, 15 μm alone and 7 + 15 μm sources not associated at all with DENIS sources are 21, 32 and 18. However, most of these 7 + 15 μm sources are not in the DENIS catalogue because they are too strong and above the saturation limit; 13 of them are present in the 2MASS data. Most (18) of the sources of 7 μm alone are also associated with 2MASS sources with $K_s \lesssim 11.0$, so that the proportion of 7 μm sources not associated with a near-IR source is negligible (~0.4%). On the other hand, only four sources of 15 μm alone are associated with 2MASS sources with $K_s \lesssim 11.0$; it results in a more important, but still small, fraction (~2%)

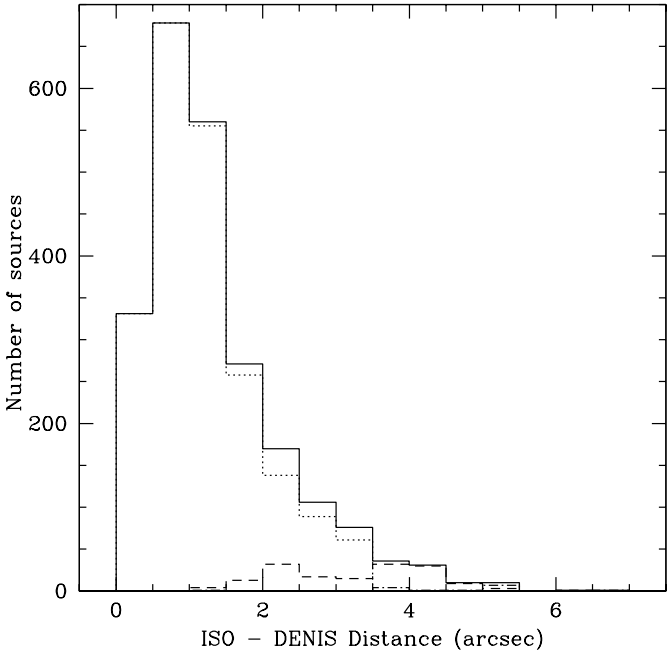

Fig. 4. Histogram of positional difference (in arcsec) between ISOGAL and DENIS cross-identified sources. Solid line shows all ISOGAL/DENIS sources. Dotted line shows the sources having ISOGAL/DENIS association quality flags 4 and 5. Dashed line shows the sources having quality flags 2 and 3. Dotted-dashed line shows the sources having quality flag 1. Associations with quality flag 1 and those with a distance larger than 5″ have been finally discarded.

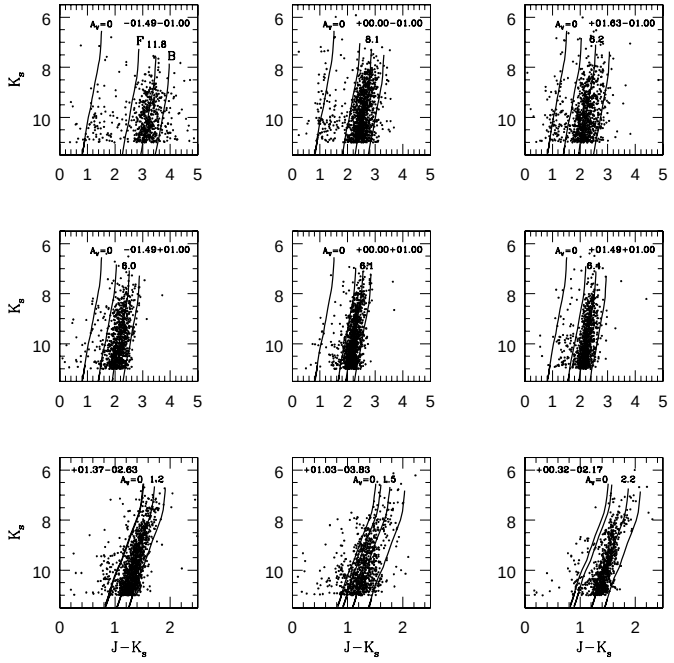

Fig. 5. Colour-magnitude diagrams ($J-K_s/K_s$) of DENIS sources in the ISOGAL intermediate bulge fields. The four isochrones (Bertelli et al. 1994), placed at 8 kpc distance for a 10 Gyr population with $Z = 0.02$ are shown in each figure for $A_V = 0$ mag, for the A_V limit adopted for the "foreground" sources (defined as "F" in top left box), for mean A_V values of the field and for the A_V limit adopted for the "background" sources (defined as "B"), respectively.

of 15 μm sources without near-IR associations, especially for the sources detected only at 15 μm (~23%). The latter could be young stellar objects (YSOs, Sect. 6.2); however, half of them have poor quality flags which could be characteristic of the spatial extension of YSOs (Schuller et al., in preparation) or cast a doubt on the reality of unassociated sources. Finally, taking into account the 15+12 rejected associations, the percentage of ISOGAL sources with a near-infrared association is larger than 97%.

4. Interstellar extinction and foreground disk stars

4.1. Interstellar extinction

The adjunction of DENIS and 2MASS near-infrared data adds much to ISOGAL data, by providing different and more sensitive colour indices, as well as estimates of the interstellar reddening. The $K_s/J-K_s$ magnitude-colour diagrams of DENIS sources in the bulge fields show a well-defined red giant sequence shifted by fairly uniform extinction (see Fig. 5), with respect to the reference K_{s0} vs. $(J-K_s)_0$ of Bertelli et al. (1994) with $Z = 0.02$ and a distance modulus of 14.5 (distance to the Galactic Center: 8 kpc). The near-infrared colours of this isochrone have been computed with an empirical $T_{\rm eff} - (J-K)_0$ colour relation built by making a fit through measurements for cool giants (see Schultheis et al. 1998, 1999). We have assumed that $A_J/A_V = 0.256$; $A_{K_s}/A_V = 0.089$ (Glass 1999). The average value of the interstellar extinction (A_V) for each bulge field is shown in Table 1 and in Fig. 5. The mean A_V value for each field has been determined by a Gaussian fit to the A_V distribution.

The DENIS sources with anomalously low values of A_V are probably foreground. They are visible in Fig. 5 in each of the bulge fields (stars around the isochrone with $A_V \sim 0$ mag and stars clearly left of the bulk of the stars grouped around the isochrone with mean A_V of the field). For each field we define an isochrone "F" (Fig. 5) for which we assume that all the sources left of it are foreground stars which will be no longer considered in the following discussions of "bulge" stars.

There are also a number of stars with $J-K_s$ values significantly larger than the bulk of the other stars in each bulge field (right of the isochrone defined as "B" in Fig. 5). We can see three reasons for such an excess in $J-K_s$: 1) intrinsic $(J-K_s)_0$ excess induced by a large mass-loss, which should be accompanied by a large 15 μm excess; 2) excess in A_V which should probably be due to a patchy extinction on the bulge line of sight (additional extinction from dust layers behind the Galactic Center for background stars appears unlikely at such high galactic latitudes); 3) spurious association or wrong photometry which is rather unlikely for DENIS sources well above the detection limit.

For the stars with such large values of $J-K_s$, right of the isochrone "B" in Fig. 5, we distinguish: a) bright stars, with $K_s < 8$, which can be bulge AGB stars with large mass-loss, for which we again use the mean extinction correction A_V of the field; and b) faint stars, with $K_s > 8$, for which we

assume low mass-loss and large extinction and we determine their specific extinction from $J-K_s$ and the zero-extinction isochrone as for the bulk of bulge sources.

To summarize, for the following discussions where dereddening is essential – colour-magnitude diagrams, luminosities, mass–loss rates – we have applied the following prescriptions: We have discarded all sources left of curves "F" in Fig. 5. For the others, with J and K detections, besides the few exceptions mentioned above, we have determined their specific extinction from $J-K_s$ (with Glass 1999 values for A_J/A_V and A_{K_s}/A_V) and the quoted zero-extinction isochrone of M giants. For all the others, especially with no JK associations, we have used the mean extinction A_V of the field (Table 1). The extinction ratios $A_{[7]}/A_V$ and $A_{[15]}/A_V$ in the ISOGAL bands are still uncertain (Hennebelle et al. 2001; Jiang et al. 2003). We have used the values $A_{[7]}/A_V = 0.020$; $A_{[15]}/A_V = 0.025$ recommended by Hennebelle et al. for "disk" fields; however, the extinction corrections remain small with the low values of A_V considered, and the effects of the uncertainty on $A_{[7]}$ and $A_{[15]}$ are practically negligible.

4.2. Proportion of foreground and background disk stars

It is clear that the method discussed above for identifying foreground stars from the value of $J-K_s$ and the inferred extinction, fails to recognize foreground disk stars located between the last dust layers and the bulge. Similarly, the extinction gives no way of distinguishing background disk stars, beyond the bulge, from bulge stars.

In order to derive an order of magnitude of the proportion of such foreground and background disk stars, mixed with bulge stars with similar extinction, one can use any reasonable simple galactic model for the M–K giants of the bulge and the disk, e.g. the one by Wainscoat et al. (1992). In Appendix A, we have thus estimated the approximate fraction of counts expected from the bulge, the disk $r < R_0$, and the disk $r > R_0$, as being about 65%, 23% and 12%, respectively, on a typical line of sight for our fields, $l = 0$, $b = 2^\circ$ (R_0 is the distance to the Galactic Center).

Indeed, stars of the actual bulge and of the central disk are indistinguishable in our analysis. We should thus consider as really foreground and background, only disk stars outside of the bulge radius $R_1 = 2$ kpc of Wainscoat et al. (1992). Their fractions are only about 14% and 6% respectively. However, part of the foreground stars have already been identified from the low value of their extinction (Sect. 4.1) and taken out of the stars further discussed below. Their number is 110, i.e. about 8% of the total.

To summarize, one may expect that the sample of ISOGAL sources further discussed below contains about 6% of foreground disk stars, 6% of background disk stars, and 88% of central stars within the bulge limits – ∼70% of bulge stars and ∼18% of central disk stars. However, these percentages must be considered as indicative since they vary with the galactic coordinates and they result from approximate estimates with a sketchy axisymmetrical bulge model.

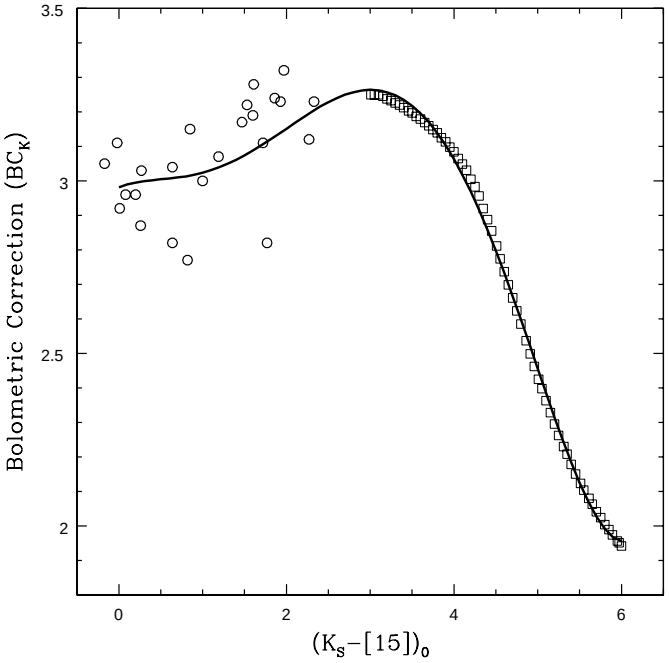

Fig. 6. Approximate relation between bolometric correction, BC_K, versus $x = (K_s–[15])_0$ ($BC_K = 2.982 + 0.0962x–0.1653x^2 + 0.1499x^3–0.04173x^4 + 0.003351x^5$) derived using the BC_K values from Frogel & Whitford (1987) (open circles) and Groenewegen (1997) (open squares) (see in the text).

5. Luminosities

After dereddening (Sect. 4.1), the bolometric magnitudes (M_{bol}) are derived for the stars using the bolometric corrections (BC_K) and a distance modulus of 14.5. We have used an approximate relation (Fig. 6) between BC_K vs. $(K_s–[15])_0$ to derive the bolometric corrections for the ISOGAL sources by combining the BC_K values derived as follows from Frogel & Whitford (1987) and from Groenewegen (1997). For $(K_s–[15])_0 < 3$, we have used 24 ISOGAL Baade's Windows sources (shown by open circles in Fig. 6) which are common in Frogel & Whitford's (1987) catalogue with a value for BC_K, to derive the average curve displayed in Fig. 6. We have extended this curve for $(K_s–[15])_0 > 3$ from the approximate relation between BC_K vs. $(K–[12])_0$ for IRAS AGB stars proposed by Groenewegen (1997). For this purpose, we have used an approximate empirical relation between $y = (K–[12])_0$ and $x = (K_s–[15])_0$ – namely, $y = x - (x/7)^3$ – derived from the modelling of infrared emission of nearby oxygen-rich AGB stars (Groenewegen, private communication). The BC_K values from Groenewegen (1997) are shown as open squares in Fig. 6. However, they have been slightly rescaled by adding 0.25 mag to match them with Frogel & Whitford's values for $(K_s–[15])_0 \lesssim 3$. Finally, a polynomial fit has been performed between BC_K and $x = (K_s–[15])_0$ (see caption of Fig. 6). We have checked that such a simple approximate determination of M_{bol} agrees within a few tenths of magnitude with an elaborate integration of all DENIS and ISOGAL flux densities along the method of Loup et al. (in preparation).

The luminosity of each star is derived from M_{bol} using the classical relation, $L(L_\odot) = 10^{-(M_{bol}-4.75)/2.5}$, and is available

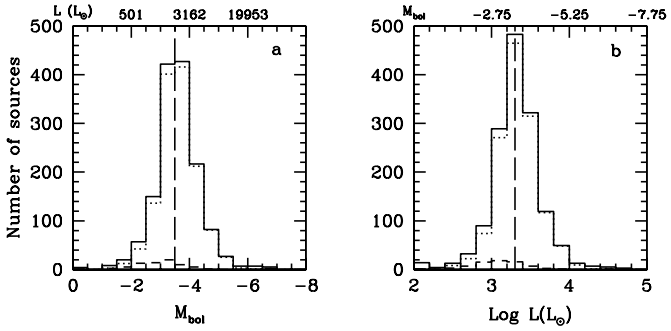

Fig. 7. Histograms showing bolometric magnitudes and luminosities of the sources in ISOGAL bulge fields. Solid lines show all ISOGAL sources detected at K_s and 15 μm. Dotted lines show the sources having ISOGAL/DENIS association quality flags 4 and 5. Short-dashed lines show the sources having quality flags 2 and 3. Long-dashed vertical lines indicate the bulge RGB tip ($M_{bol} \sim -3.5$; $L \simeq 2000\ L_\odot$).

in Table 2. Figures 7a, b show the histograms of bolometric magnitudes and luminosities of the sources in ISOGAL bulge fields. These distributions are clearly incomplete below the luminosity of the bulge RGB tip. One should keep in mind that for ∼12% of the sources, the luminosities thus derived are wrong because their distances are significantly different from the bulge distance, either foreground or background on the line of sight. This will spuriously broaden the luminosity distribution. In particular, most of the sources appearing with very large luminosities are probably foreground stars with smaller luminosities. In addition, even for the other sources within the "bulge" limits (6–10 kpc), the difference in distances with respect to 8 kpc induces a spread by about one magnitude (but with an rms $\lesssim 0.2$ mag because the distribution is very centrally peaked). Other uncertainty terms, to be combined in quadrature, include the residuals to the BC_K fit and the BC_K calibration (rms $\lesssim 0.2$ mag), uncertainties in the K and 15 μm photometry (rms $\lesssim 0.2$ mag), dereddening for large extinctions (rms < 0.2 mag), variability (rms ~ 0.2 mag for strong variables, <0.1 mag for others). The combined rms uncertainty for the luminosity of bulge sources is thus probably less than 0.4–0.5 mag.

6. Nature of the ISOGAL sources

Figures 8, 9 and 11 show the $(K_s–[15])_0/[15]_0$, $(K_s–[15])_0/K_{s0}$ and [7]–[15]/[15] colour-magnitude diagrams of ISOGAL sources, respectively. The first two diagrams are more directly related to the luminosity and mass-loss derivations (Sects. 5 and 7), and luminosity and mass-loss rates estimate are displayed in Figs. 8 and 9. However, such derivations rely on a good extinction correction of K_s magnitudes. On the other hand, the diagram [7]–[15]/[15], which depends little on extinction, provides a straightforward view of the nature and the amount of dusty sources of various classes. It even allows a direct measure of the mass-loss rates, but with less sensitivity, especially for the largest and the smallest ones.

Figures 8, 9 and 11 are very similar to the same diagrams in Omont et al. (1999) for the field at $l = 0$, $b = +1^\circ$ (see also Glass et al. 1999). One can distinguish three main classes of

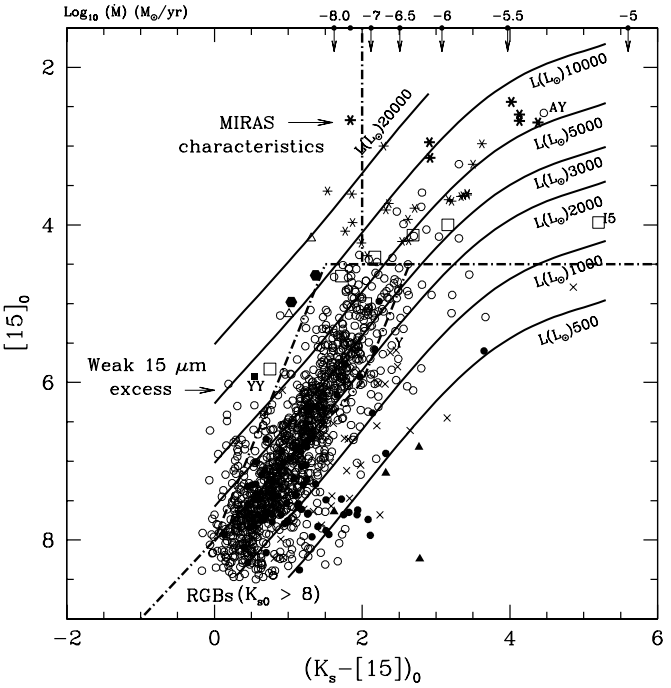

Fig. 8. [15]/K_s–[15] magnitude-colour diagram of ISOGAL sources with DENIS/2MASS counterparts. The open circles show the sources having ISOGAL–DENIS association quality flags of 4 and 5. The crosses show the sources having association quality flags of 2 and 3 (see the text). The filled hexagons display the ISOGAL sources associated with 2MASS counterparts (since the DENIS sources [$K_s \leq 6.5$] are saturated, they have been replaced by the 2MASS sources). The remaining saturated DENIS sources (which have no published 2MASS counterparts) are shown by filled squares. The bright ISOGAL sources associated with 2MASS sources (which have no DENIS counterparts) are shown by open triangles. Sources without 7 μm associations are displayed by filled circles. The filled triangles show the ISOGAL sources associated with 2MASS sources but having no DENIS counterparts. The IRAS sources are shown by open squares. However the four very red IRAS sources I1–4 (Table 3) are outside the limits of the figure. The asterisks show the sources detected at 8 μm in the MSX survey which are associated with strong ISOGAL sources ([15] < 4.5 mag). Among them the dark ones are those associated with the MSX D (15 μm) sources ([15] < 3.5 mag). The curves from bottom to top represent the luminosity estimates from 500 to 20 000 $L_\odot$, respectively (see Fig. 5). Various regions discussed in the text (see Sect. 6) are indicated with boundaries as dotted lines. The approximate scale of mass-loss rate displayed at the top of the figure is derived from Eq. (1) given by Jeong et al. (2002) (see Sect. 7).

sources, corresponding to three regions delimited in Figs. 8, 9 and 11.

There are first, a number of stars with luminosity (<2000 $L_\odot$) and colours [$(K_s–[15])_0 < 1$] and [7]–[15] consistent with dustless stars on the RGB close to its tip, which is at $K_0 \sim 8.0$ as quoted by Frogel et al. (1999)[2], which corresponds to $M_{bol} \simeq -3.5$ and $L \simeq 2000\ L_\odot$. Their spectral types should be ∼M3–M5 (Frogel & Whitford 1987; Glass et al. 1999), which corresponds to colour $(K_s–[15])_0 \simeq 0.71–0.78$ with $T_{eff} \simeq 3600–3400$ K, respectively.

[2] As quoted in footnote 2 of Omont et al. (1999), we neglect the small difference of $K–K_s \sim 0.04$, for such stars.

Then, a whole sequence of sources display luminosities slightly above the RGB tip (2000–5000 $L_\odot$) and colours with a weak 15 μm excess [1 < $(K_s$–[15])$_0$ < 2], characteristic of small amounts of dust and thus of weak mass–loss; they were called "intermediate AGB" stars by Omont et al. (1999). The K_{s0} magnitude range from the base to tip of the sequence (Fig. 9) corresponds to M spectral types from about M6 to M8–M9 (Frogel & Whitford 1987; Glass et al. 1999). It is known from Alard et al. (2001) that they are semi-regular variables with relatively short periods and weak amplitudes.

Finally, less numerous sources, in the top right corner of Figs. 8 and 11 ([15]$_0$ < 4.5, $(K_s$–[15])$_0$ > 2, ([7]–[15])$_0$ $\gtrsim$ 1.3), may have larger luminosities and super–wind mass–loss characteristic of Miras (see Glass et al. 1999; Alard et al. 2001; Omont et al. 1999). Most of them are detected at 8 μm in the MSX survey (Price et al. 2001) as seen in Table 2.

6.1. Brightest and reddest ISOGAL sources

We have identified 16 IRAS sources within the fields of Table 1. They are associated with 15 bright ISOGAL stars ([15]$_0$ $\lesssim$ 6.0). Table 3 shows the brightest and reddest ISOGAL sources with IRAS and MSX associations when available. These sources are shown by open squares in Figs. 8, 9, 11 and 12. Out of these 15 sources, the four brightest ones ([15]$_0$ < 1.5) are denoted by "I1–4" in Table 3 and Figs. 9 and 12. These four sources visible in Figs. 9 and 11 are not shown in Figs. 8 and 12. All of them have extremely red values of $(K_s$–[15])$_0$ characteristic of large amount of dust. Their [12]–[25] IRAS colours are characteristic of AGB stars and not of young stellar objects or post-AGB stars. They are thus probably AGB stars with very large mass-loss rates, $>10^{-5}$ $M_\odot$ yr^{-1} (see Sect. 7 and Table 3). Table 3 displays approximate values of their bolometric fluxes computed from an integration of their available flux densities, either following the prescriptions of Loup et al. (in preparation) or from a more approximate integration when $(K_s$–[15])$_0$ is too large to use Loup et al's method. All of them correspond to large values of bolometric luminosities if the sources are at the Galactic Center distance. Such luminosity values are consistent with the very large mass-loss rates and both quantities point out to relatively large values of the initial mass. However, it is not clear whether these stars belong to the central bulge/disk or to the foreground disk (the four of them have $|b| \simeq 1$). Their large intrinsic colours make it very difficult to determine their interstellar extinction. Their following individual properties may help to decide about their bulge membership:

– **I1** – It is the brightest 15 μm source and its ISOGAL magnitudes are uncertain because of saturation. It belongs to the most extreme class of OH/IR stars with a massive cold circumstellar envelope as shown by its exceptional [12]–[25] colour and strong 10 and 18 μm absorption bands in the IRAS LRS spectrum (IRAS Science Team 1986). The radial velocity and the very large bolometric flux point to a foreground disk object.

– **I2** – The bolometric flux favours bulge membership.

– **I3** – It is also an OH maser, but its radial velocity and relatively small bolometric flux point to bulge membership.

– **I4** – The bolometric flux and the blue [7]–[15] colour favour foreground disk membership.

Three other stars with very red [7]–[15] colours (Fig. 11) are also listed in Table 3. Their nature – AGB, post–AGB, PN, YSO – is uncertain, and they are not detected by MSX. We have also added an IRAS source, YY, with no ISOGAL point source counterpart:

– **I5** – From its position in the [7]/[7]–[15] diagram, it could be either a young stellar object (YSO) or an AGB star (Schuller et al., in preparation). However, its non detection at 12 μm together with the large value of the ratio $S_{25_{\mu m}}/S_{15_{\mu m}} \sim 6$, and its small bolometric flux could indicate a young stellar object (or a planetary nebula).

– **AY** – Again, from its position in the [7]/[7]–[15] and $K_{s0}/(K_s$–[15])$_0$ diagrams, and from its bolometric flux, it could be a YSO or an AGB star.

– **Y** – It could appear as a good YSO candidate. However, its ISOGAL magnitudes could have been affected by the track of the saturated star I1 in the ISOGAL images. Its completely anomalous colour $(K_s$–[7])$_0$ = −0.15 also points to a wrong 7 μm magnitude.

– **YY** – This source, IRAS 17423–3048, is probably a massive YSO from its IRAS 25–60 μm flux densities. It has no convincing association in the ISOGAL-DENIS PSC, although the ISOGAL–DENIS–MSX source displayed within bracketts in Table 3 is within the limits of a possible association. On the other hand, there is some extended emission at its position in the 15 μm ISOGAL image.

6.2. Other detected sources

All other IRAS detected sources have [12]–[25] colours indicative of AGB stars. The fact that there are practically no other stars in Fig. 11 meeting the criteria ([7]–[15] > 1.8 with [15] < 4.5) for credible young star candidates defined by Felli et al. (2000, 2002), is not surprising in such high galactic latitude lines of sight.

As quoted in Glass (1999), much of the scatter (∼1 mag) seen in the "AGB sequence" of Figs. 8 and 11) may be due to the distribution in the depth of the bulge and the central disk (Glass et al. 1995). Furthermore, in Figs. 8 and 9, it seems unlikely that there is in addition an anomalously large number of stars far above this sequence by up to ∼1.5 mag. Such stars with anomalously bright ISOGAL magnitudes with respect to their colours, appear more clearly in the [7]–[15]/[15] colour/magnitude diagram of Fig. 11. It seems that most of them could not be bulge AGB stars with very high luminosity, because of the age of the bulge population and of the low mass-loss rates deduced for most of them from $(K_s$–[15])$_0$ or [7]–[15]. Most of them are probably foreground AGB stars with moderate luminosity and mass-loss. Their population and the distribution of the values of the 15 μm magnitude excess with respect to the bulge sequence look in rough agreement with the proportion and the distance distribution expected for the disk foreground stars (Sect. 4). Similarly, most sources which lie below the main bulge AGB sequence in Figs. 8, 9 and 11, are likely background disk AGB stars.

Table 3. Catalog of brightest and reddest ISOGAL sources. Data for each source are displayed in two lines, with the ISOGAL standard name (e.g. ISOGAL-PJ173812.5-293938) and the IRAS name if any. In order to make the easy comparison with ISOGAL 7 and 15 μm magnitudes, [7] and [15], and IRAS flux densities (in Jy) at 12 and 25 μm, S12 and S25, MSX intensities are given in magnitudes for bands A (~8 μm) and D (~15 μm), and in flux densities (in Jy) for bands C (~12 μm) and E (~21 μm).

Name (ISOGAL–P..) IRAS Name	l b (deg)	J (mag)	K_s (mag)	[7] msx$A$ (mag)	[15] msx$D$ (mag)	A_V (mag)	V^1_{LSR} (km s^{-1})	S12 msx$C$ (Jy)	S25 msx$E$ (Jy)	L^2 10^4 $L_\odot$	$\dot{M}$ ($M_\odot$ yr^{-1})	Id.
J173812.5-293938	−1.5	11.75	8.16	5.26	2.89	6.3				0.32	4.9×10^{-6}	AY
	1.0											
J174122.7-283146	−0.1	>14.16	11.80	3.47	1.54	8.9	−51.0	2.0	4.3	0.89	3.2×10^{-5}	I3
17382-2830	1.0			3.69	1.87			2.5	4.7			
J174458.5-271442	1.4	12.83	10.80	0.90	−0.51	6.1	−12.3	15.0	51.3	8.87	4.1×10^{-5}	[3]I1
17418-2713	1.0			1.21	−1.28			31.2	80.3			
J174506.1-271516	1.4	10.92	8.67	8.43	5.84	5.4				0.16	2.9×10^{-7}	Y
	1.0											
J174522.9-271109	1.5	>15.88	12.50	2.65	1.42	8.0		4.5	4.9	3.67	3.6×10^{-5}	I4
17422-2709	1.0			2.74	1.23			4.6	5.7			
(J174533.2-304943)	1.6	(11.13)	(7.64)	(6.66)	(6.13)	(11.9)			1.6:	0.66		YY
17423-3048	−1.0			(6.07)								
J174548.6-304312	−1.5	>15.26	10.14	4.38	1.58	12.3		3.4	5.3	0.17	1.7×10^{-5}	I2
17426-3042	−1.0			3.67	1.85			2.7	4.2			
J174939.4-292723	0.0	12.31	9.85	6.34	4.16	7.6			2.5	0.12	8.1×10^{-6}	I5
17464-2926	−1.0											

[1] Value comes from OH maser detection.
[2] If one assumes a distance of 8 kpc.
[3] The ISOGAL magnitudes and M_{bol} of I1 are uncertain because the ISOGAL flux densities are above saturation limits of the detectors.

There are a few stars (Fig. 9) with large values of $(K_s–[15])_0$ (>1) below the RGB tip. But their case is not clear. Only a few of them have values of $([7]–[15])_0 > 0.6$. Most of the sources have poor photometry because they are close to the 15 μm detection limit or of poor association quality. In the following discussion, we will drop the most doubtful cases, i.e. all stars with $K_{s0} > 9.0$ (Fig. 9). The nature of the few remaining cases is unclear. A number could be background stars with large mass-loss. Additional observations are required to confirm the nature of these sources and to exclude the possibility of spurious associations with the K_s sources. However, such a 15 μm excess could be an indication that some RGB stars close to the RGB tip have a significant mass-loss, as found in globular clusters by Origlia et al. (2002).

The 28 sources detected only at 15 μm (Sect. 3) are absent from all colour–magnitude diagrams. However, they remain candidates for YSOs or Planetary Nebulae, especially for half of them with relatively good quality flags. The strongest one, ISOGAL–PJ1753178–280433, [15] = 5.88, is identified in SIMBAD as a Planetary Nebula JaSt 90 (van de Steene & Jacoby 2001).

Figure 12 shows $[7]/K_s$–[7] magnitude-colour diagram of ISOGAL sources. The $[7]/K_s$–[7] diagram seems to be the best criterion for the detection of large amplitude LPVs (Glass et al. 1999; Schultheis et al. 2001). The region of high mass-loss AGB stars ($(K_s–[7])_0 > 1$, $[7]_0 < 7$) is explicitly drawn in this diagram.

7. Mass-loss rate ($\dot{M}$) determination

It is generally agreed that the colour $(K–[12])_0$ (where [12] is the magnitude corresponding to the IRAS 12 μm flux density) is a good indicator of the mass-loss rate $\dot{M}$ of AGB stars (see e.g. Whitelock et al. 1994; Le Bertre & Winters 1998; Jeong et al. 2002). It is clear that $(K_s–[15])_0$ should be an equally good gauge of $\dot{M}$, with a slightly different calibration. However, the relation between $\dot{M}$ and $(K_s–[15])_0$ or $(K–[12])_0$ directly depends on the nature of dust and on the gas-to-dust ratio. For instance, there is evidence from the preliminary analysis of the ISOGAL CVF data of a few of these AGB bulge sources that their dust is dominated by alumina for low and intermediate mass-loss rates (Blommaert et al. 2001 and in preparation). In addition to further analysis and observations of mid–IR spectra, an essential element for the accurate calibration of the relation between $\dot{M}$ and $(K_s–[15])_0$ is the detailed theoretical analysis of mass-loss physics, dust formation and radiative transfer, such as performed by Jeong et al. (2002 and in preparation). The latter is based on a consistent time dependent treatment of hydrodynamics, thermodynamics, equilibrium chemistry and dust formation. Such a theoretical modelling is presently the only way to infer the gas-to-dust ratio and the mass-loss rates for such bulge sources in the absence of any direct measurement of the mass of circumstellar gas and even of the expansion velocity. As they quote, the relation derived between $\dot{M}$ and $(K–[12])_0$ by Jeong et al. (2002) gives substantially higher mass-loss rates than the empirical relation of

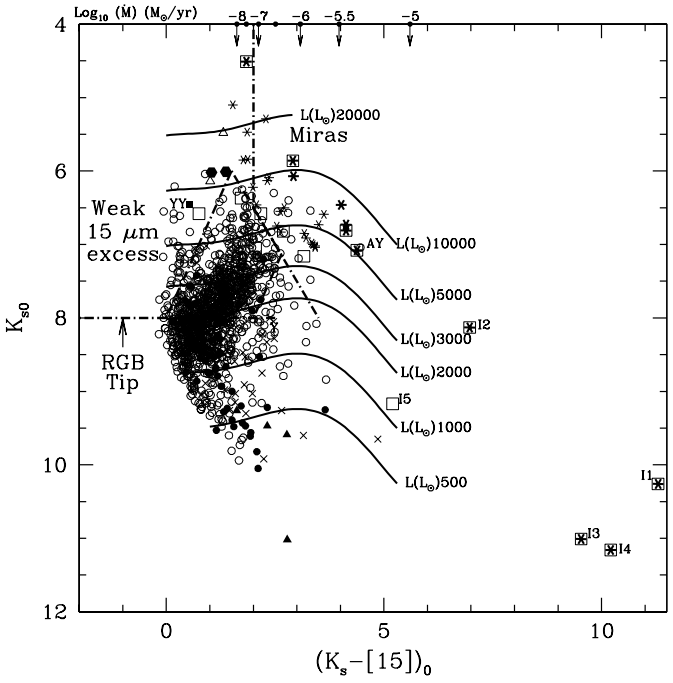

Fig. 9. $K_{s0}/(K_s–[15])_0$ magnitude-colour diagram of ISOGAL sources with DENIS/2MASS counterparts. The symbols and the curves are same as shown in Fig. 8. The red IRAS sources of Table 3 are denoted by "I" (see text). They are also MSX D sources associated with the strong 15 μm sources. The RGB tip ($K_{s0} \sim 8.0$) is shown as dotted line. The other two regions are the same as in Fig. 8.

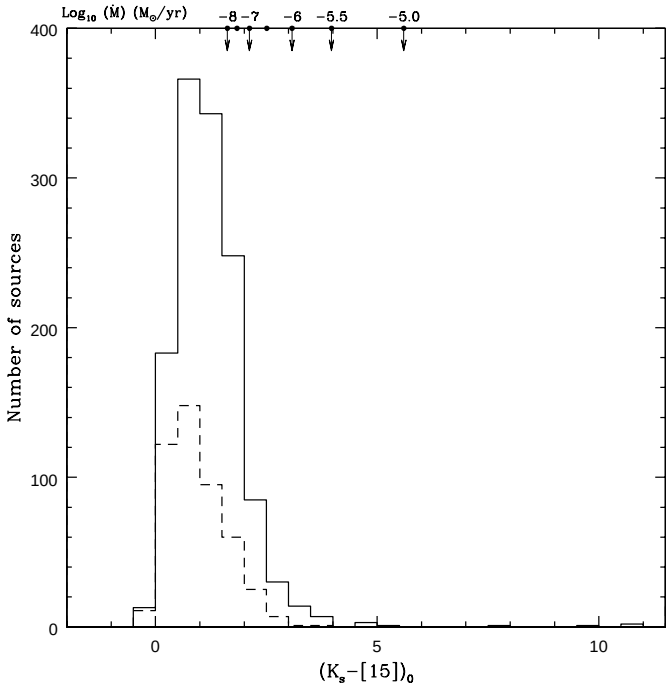

Fig. 10. K_s–[15] colour distribution of ISOGAL sources. The mass-loss scale at the top of the figure are same as shown in Fig. 8. The full line histogram represents the stars of all nine fields of our sample (Table 1). The dashed line represents stars in the fields with $|b| \geq 2°$.

Le Bertre & Winters (1998) (Fig. 13). On the other hand, the agreement is better with the empirical values of Whitelock et al. (1994) derived from the classical prescription of Jura (1987) giving $\dot{M}$ from far-infrared emission (Fig. 13). Here, we will apply the explicit relation between $\dot{M}$ and $(K–[15])_0$ derived by Jeong et al. (2002),

$$\log\dot{M} = -6.83/(K–[15])_0 - 3.78 \quad (1)$$

with $\dot{M}$ in $M_\odot$ yr^{-1} (Fig. 13).

Alternatively, one could also infer $\dot{M}$ from $(K_s–[7])_0$ or from [7]–[15]. Deriving $\dot{M}$ from [7]–[15] (Alard et al. 2001) has the advantage that the latter quantity depends very little on the extinction. However, this method is less sensitive since [7]–[15] varies little. On the other hand, $(K_s–[7])_0$ has a low sensitivity for small mass-loss rates, but could be conveniently used for large ones.

It is important to notice that there may also be an appreciable uncertainty in the determination of mass-loss rates from $(K–[15])_0$ for strongly variable stars where we have only single epoch measurements of K_s and [15], and at different epochs for K_s and [15] (Table 1). As quoted, this uncertainty is reduced by taking the average of DENIS and 2MASS K_s values and of ISOGAL and MSX 15 μm magnitudes. One can thus estimate that the global rms uncertainty on $(K_s–[15])_0$ remains smaller than 0.3–0.4 mag, except for the weakest sources ($K_{s0} > 9.0$, see Sect. 6.2). However, because of the rapid variation of $\dot{M}$ versus $(K_s–[15])_0$ (Fig. 13), the corresponding observational uncertainty on $\dot{M}$ ranges between a factor ∼2 for its largest values $>10^{-6}$ $M_\odot$ yr^{-1}, and ∼5 for the smallest ones $<10^{-7}$ $M_\odot$ yr^{-1}. Such values do not include the model uncertainty in the relation between $\dot{M}$ and $(K_s–[15])_0$.

8. Total mass-loss rate in the bulge

Figure 14a shows the number distribution of mass-loss rates ($\dot{M}$) of ISOGAL sources in the bulge as a function of $\dot{M}$ from Eq. (1) along models of Jeong et al. (2002). Figure 14b displays the corresponding values of the average total mass-loss rate per square degree and per 0.5 bin of log $\dot{M}$. It should be remembered that the number of sources is incomplete for $\dot{M} \lesssim 10^{-7}$ $M_\odot$ yr^{-1}. It is not excluded that still lower mass-loss rates, $\dot{M} < 10^{-8}$ $M_\odot$ yr^{-1}, contribute a little to the integrated mass-loss in the bulge, because of the very large number of stars with $1 \lesssim (K_s–[15])_0 \lesssim 2$ (Fig. 10), where such 15 μm excess, if real, still shows the presence of circumstellar dust.

However, because of the very steep distribution of the number of sources versus $(K_s–[15])_0$ (Fig. 10) and the rapid variation of $\dot{M}$ versus $(K_s–[15])_0$ (Fig. 13), the error in $(K_s–[15])_0$ due to strong variability makes the contribution of the corresponding bins larger than in reality. Therefore, in Figs. 14b, d, we have reduced the contributions of the three bins between 10^{-7} and 3×10^{-6} $M_\odot$ yr^{-1} by factors 1.4, 1.2 and 1.1, respectively, as shown in Figs. 14a, c. However, we have not corrected the bins below 10^{-7} $M_\odot$ yr^{-1}, because the incompleteness of detections of such stars could compensate for this effect.

It is difficult to fully appreciate the uncertainty in the data of Figs. 14a, b. There are various sources of observational uncertainty: errors in $K_s–[15])_0$ and their uncertain correction, bulge membership, Poisson error due to the small number of

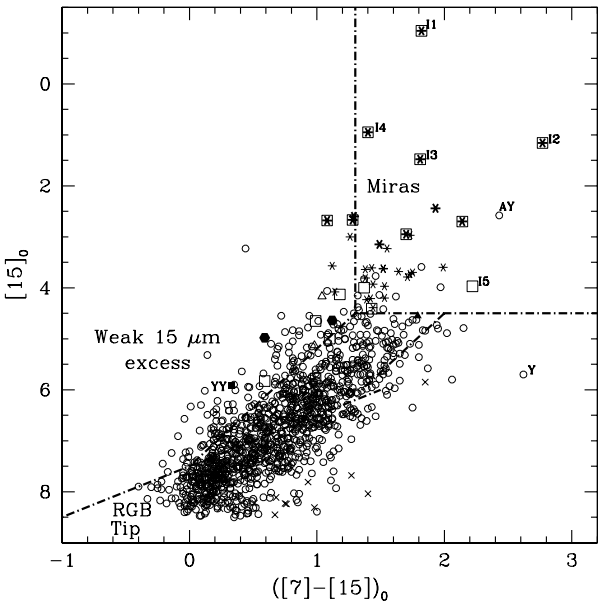

Fig. 11. [15]/[7]–[15] magnitude-colour diagram of ISOGAL sources detected in the ISOGAL fields. The open circles show the ISOGAL sources having 7/15 μm association quality flags of 3 and 4. The crosses show the sources having association quality flags of 2. The filled hexagons display the associations with 2MASS (since the DENIS sources [$K_s \leq 6.5$] are saturated, they have been replaced by 2MASS). The remaining saturated DENIS sources (which have no 2MASS counterparts) are shown by filled squares. The bright ISOGAL sources associated with 2MASS sources (which have no DENIS counterparts) are shown by open triangles. The filled triangles show the ISOGAL sources which have no available DENIS nor 2MASS counterparts, mostly because of saturation or non observation. The asterisks show the sources detected at 8 μm in the MSX survey which are associated with strong ISOGAL sources ([15] < 4.5 mag). Among them the dark ones are those associated with the MSX D (15 μm) sources ([15] < 3.5 mag). The IRAS sources are shown by open squares and the brightest ones are denoted as "I" (see text). Sources with larger luminosities and super-wind mass-loss characteristic of Miras are inside the boundaries shown as dotted lines. Other two regions are same as in Fig. 8.

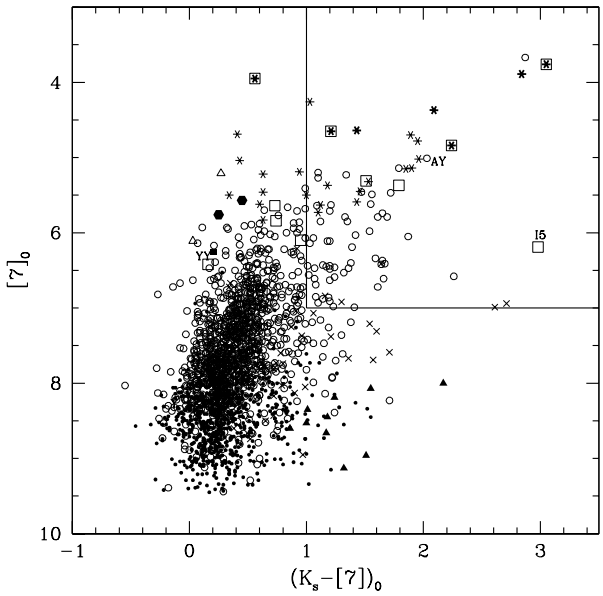

Fig. 12. $[7]_0/(K_s–[7])_0$ magnitude-colour diagram of ISOGAL sources with DENIS/2MASS counterparts. The open circles show the sources having ISOGAL-DENIS association quality flags of 4 and 5. The crosses show the sources having association quality flags of 2 and 3 (see the text). The filled hexagons display the ISOGAL sources associated with 2MASS counterparts (since the DENIS sources ($K_s \leq 6.5$) are saturated, they have been replaced by the 2MASS sources). The remaining saturated DENIS sources (which have no 2MASS counterparts) are shown by filled squares. The bright ISOGAL sources associated with 2MASS sources (which have no DENIS counterparts) are shown by open triangles. Sources without 15 μm associations are displayed by filled circles. The filled triangles show the ISOGAL sources associated with 2MASS sources but having no DENIS counterparts. The asterisks show the sources detected at 8 μm in the MSX survey which are associated with strong ISOGAL sources ([15] < 4.5 mag). Among them the dark ones are those associated with the MSX D (15 μm) sources ([15] < 3.5 mag). Stars I1–4 are outside of the figure limits with $(K_s–[7])_0$ between 4 and 10 (see Table 3). The region of high mass-loss AGB stars ($(K_s–[7])_0 > 1$, $[7]_0 < 7$) is drawn in the upper right corner (see Fig. 9 of Omont et al. 1999).

sources with large $\dot{M}$, incompleteness of detections of stars with small $\dot{M}$, etc. They could combine to give a substantial error, but probably smaller than a factor two. However, the major source of error is probably still the calibration of the relation between $K_s–[15])_0$ and $\dot{M}$, which depends on dust properties and the dust–to–gas ratio. Its modelling depends on complex stellar properties and remains difficult despite the spectacular progress achieved by Jeong et al. (2002).

It is seen in Fig. 14b that the contribution to the integrated mass-loss per bin of log $\dot{M}$ is dominated by mass-loss rates larger than 10^{-6} $M_\odot$ yr^{-1}. It is even possible that the four stars I1–4 with $(K_s–[15])_0 > 6$, $\dot{M} \gtrsim 10^{-5}$ $M_\odot$ yr^{-1} (Table 3), contribute for about half the total. But their belonging to the bulge is not fully established (see Sect. 6).

Numerical values for the integrated mass-loss are displayed in Table 4. First are values for mass-loss per square degree averaged over all nine fields of Table 1, with and without including the contribution of the four stars I1–4, respectively. Since it is difficult to decide whether such stars belong to the central bulge/disk or not (Sect. 6.1), we also give the same quantities for the three fields with $|b| > 2°$ where such stars with very large values of $\dot{M}$ ($(K_s–[15])_0 > 4$) are absent (see Fig. 10). The corresponding distribution of mass-loss rates are displayed in Figs. 14c, d. In the absence of stars with $(K_s–[15])_0 > 4$, it is seen that the relative contribution of large mass-loss rates to the integrated mass-loss seems smaller. However, the total number of relevant stars with $(K_s–[15])_0 > 2$ is about four times smaller in the three fields with $|b| > 2°$ than in the totality of the fields. Therefore, while there are only four stars with $\dot{M} > 10^{-5}$ $M_\odot$ yr^{-1} in the totality of the fields, one cannot consider that their absence in fields with $|b| > 2°$ is statistically significant.

Such results seems to show that the relative contribution of stars with low mass-loss rates ($\dot{M} < 10^{-6}$ $M_\odot$ yr^{-1}) is more important in the mass return to the interstellar medium for the old bulge population, which is more predominant at $|b| > 2°$. Even the stars with $\dot{M} < 10^{-7}$ $M_\odot$ yr^{-1} may have a significant contribution.

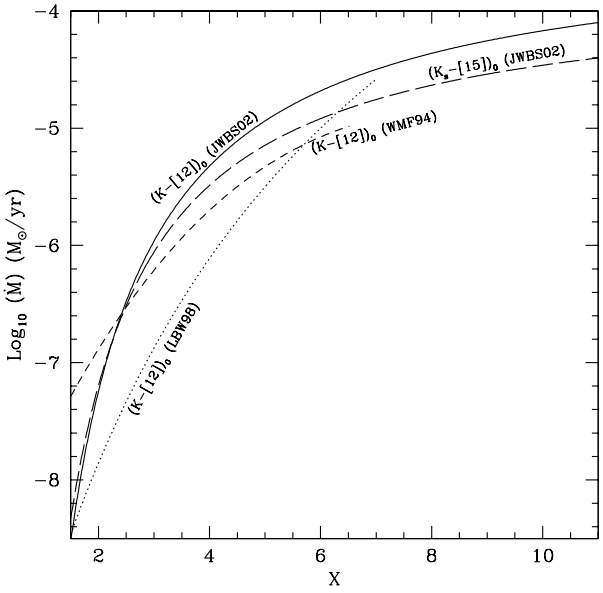

Fig. 13. Mass-loss rate ($\dot{M}$) as a function of colour. For $X = (K_s–[15])_0$, Eq. (1) recommended by Jeong et al. (2002, JWBS02) is used. For $X = (K–[12])_0$, the three curves drawn are derived from Jeong et al. (2002) with $\log_{10} \dot{M} = -7.69/(K–[12])_0) - 3.40$, Whitelock et al. (1994, WMF94) and Le Bertre & Winters (1998, LBW98), respectively.

It is not clear whether the stars with very large mass-loss rates, $\dot{M} \gtrsim 10^{-5}\ M_\odot\ \mathrm{yr}^{-1}$, which are probably younger with a relatively large initial mass, may have an essential contribution, as it seems the case for the solar neighbourhood (see e.g. Le Bertre et al. 2001). It would be interesting to make a detailed comparison with the solar neighbourhood. However, in addition to the question of bulge membership of stars with such large mass-loss in our sample, it is difficult to make a precise comparison with the recent work of Le Bertre et al. (2001) because their sample is not as complete for stars with low mass-loss as for large mass-loss ones.

We may assume the value of Eq. (A.8) for an approximate average bulge projected mass density at the average position $l = 0°$, $|b| = 2°$ for our fields, from the model of Wainscoat et al. (1992) – $\Sigma_{\mathrm{Bu}}(0, 2) \simeq 5.7 \times 10^7\ M_\odot\ \mathrm{deg}^{-2}$. We infer a rough value for the total (bulge + disk) projected mass density of $\simeq 8 \times 10^7\ M_\odot\ \mathrm{deg}^{-2}$, by assuming the same disk/bulge ratio, 30/70, as for the stellar counts estimated in the conclusion of Sect. 4.2. The derived integrated mass-loss rate per unit stellar mass is thus about $0.4–1.0 \times 10^{-11}\ \mathrm{yr}^{-1}$.

One notes that there is a difference by a large factor in the average mass-loss per square degree between the fields with $|b| > 2°$ and those with $|b| < 1.5°$. This factor is 5 and 12, without and with the contribution of stars I1–4, respectively (Table 4). On the other hand, since the bulge projected mass density varies as $[b^2+(\ell/1.6)^2]^{-0.4}$ from the model of Wainscoat et al. (1992) (see Eq. (A.7)), the corresponding ratio for the average projected mass density is only $\simeq 2$ for the bulge. It should be $\simeq 3$ when one takes into account the disk contribution. A possible explanation is that the fields closer to the Galactic Center contain a larger proportion of younger stars than in the outer bulge (Frogel et al. 1999), which, in particular, contribute more to the large mass-loss rates. However, a deeper discussion, with more elaborate Galactic models and a better identification of foreground sources, will be necessary to well establish and quantify these properties.

Table 4. Integrated mass-loss ($M_\odot$/yr/deg^2) in the "intermediate" bulge, from Eq. (1) (Jeong et al. 2002) with $\dot{M} > 10^{-8}\ M_\odot\ \mathrm{yr}^{-1}$.

	with I1-4†	without I1-4†
All fields	8.1×10^{-4}	3.7×10^{-4}
Fields with $\|b\| > 2°$	1.2×10^{-4}	1.2×10^{-4}
Fields with $\|b\| < 1.5°$	1.4×10^{-3}	5.9×10^{-4}

† Stars with $\dot{M} \gtrsim 10^{-5}\ M_\odot\ \mathrm{yr}^{-1}$ whose bulge membership is uncertain (Table 3 and Sect. 6.1).

9. Conclusion

We have analysed in detail the AGB population in the available ISOGAL "intermediate" bulge fields ($|l| < 2°$, $|b| \sim 1°–4°$). We have confirmed that the combination of near-infrared and mid-infrared (7 and 15 μm) ISOGAL data allows reliable detection of AGB stars above the RGB tip with a determination of their luminosity (providing that they belong to the bulge) and mass-loss rate. We conclude that almost all the ∼1300 ISOGAL sources detected both at 7 and 15 μm on the line of sight of the bulge are AGB stars or RGB tip stars. A large proportion of these AGB stars have appreciable mass-loss rates, as shown by the excess in $(K_s–[15])_0$ and $([7]–[15])_0$ colours, characteristic of circumstellar dust emission. We have performed a preliminary determination of mass-loss rates from $(K_s–[15])_0$ from recent theoretical modelling by Jeong et al. (2002) which are in agreement with Whitelock et al. (1994) for $(K–[12])_0$. For the bulk of our sample, and especially at $|b| \sim 1°$, the total mass returned to the interstellar medium is dominated by mass-loss rates larger than $10^{-6}\ M_\odot\ \mathrm{yr}^{-1}$. However, four stars, out of ∼2000, have mass-loss rates $\gtrsim 10^{-5}\ M_\odot\ \mathrm{yr}^{-1}$. They could dominate the mass return to the interstellar medium if they all belonged to the bulge, which is still unclear. In the more outer bulge, $|b| > 2°$, the contribution of large mass-loss rates seems less important.

Appendix A: Numbers of foreground and background disk sources

In order to derive an order of magnitude of the proportion of foreground and background disk stars, on the line of sight of the observed bulge fields, one can use any reasonable simple Galactic model for the distribution of contributing stars, e.g. the one by Wainscoat et al. (1992). We have quoted that practically all bulge sources detected by ISOGAL are M giants later than about M3. Background detected stars should be even later M giants, while the great majority of foreground disk sources are K or early M giants. It would be straightforward, but tedious, to determine the proportion of foreground and background disk stars in any given magnitude bin, on various lines of sight, by direct numerical integrations of the Galactic

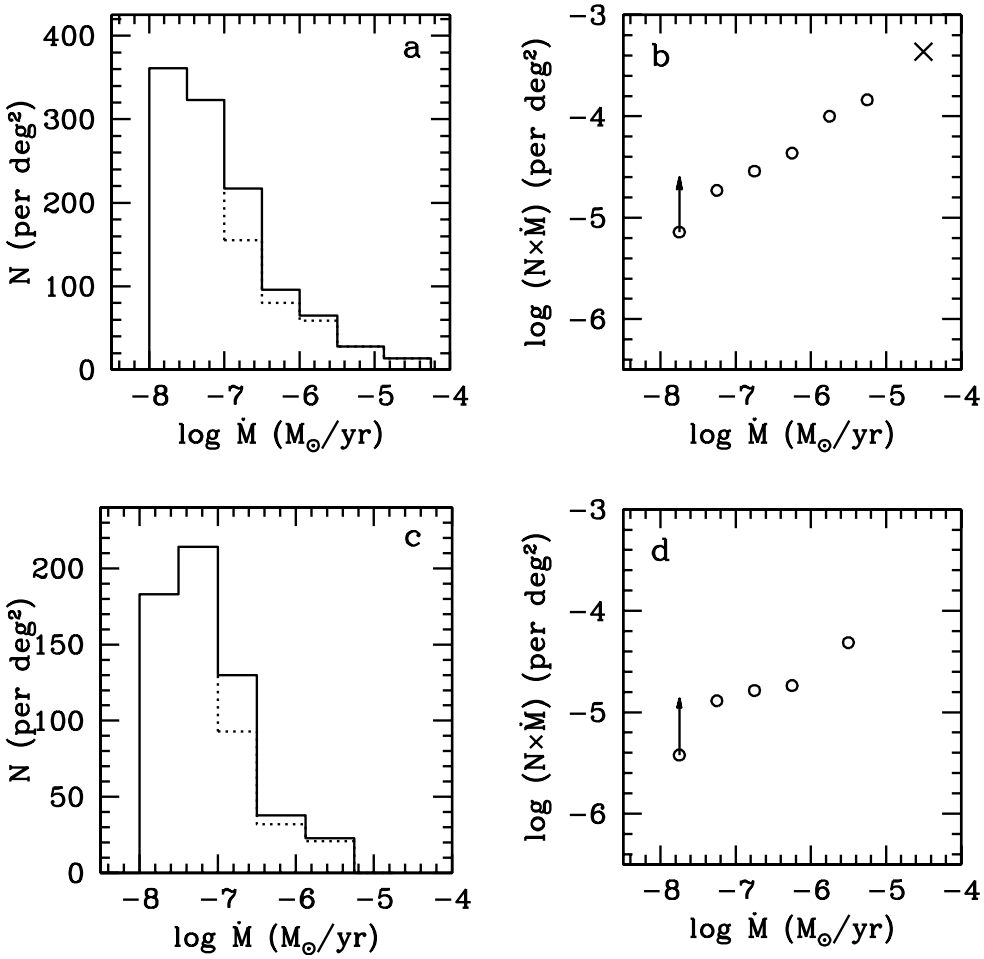

Fig. 14. a) Distribution of mass-loss rates ($\dot{M}$) of ISOGAL sources inferred from $(K_s–[15])_0$ in the nine bulge fields, derived from the formula of Jeong et al. (2002), Eq. (1). The dotted line includes a tentative correction for the spurious counts due to the error in $(K_s–[15])_0$ and the very steep count distribution, as described in the text. **b)** Average total mass-loss rate per square degree and per 0.5 bin of log ($\dot{M}$) as a function of $\dot{M}$ after this correction. The contribution of stars I1–4, $\dot{M} \gtrsim 10^{-5}\ M_\odot\ \mathrm{yr}^{-1}$, is shown by a cross. The arrow shows the incompleteness on the data for the smallest mass-loss rates. **c)** and **d)**. Same as **a)** and **b)**, but limited to the three fields with $|b| > 2$.

distributions of the various classes of stars – especially red giants – of Wainscoat et al. However, we take advantage of the simple behaviour of the giant luminosity function to make an approximate analytical integration. The K–M giant luminosity function is roughly proportional to L^{-1} (see e.g. Frogel & Whitford 1987). At the point (r, z) in the direction (ℓ, b), with $b \ll 1$ and $z = rb$, the number of such giants per unit volume and absolute magnitude bin $\mathrm{d}M_i$ is $\rho_g(r,z) \times f_i(M_i)\mathrm{d}M_i$ where $f_i(M_i)$ is approximately proportional to $10^{M_i/2.5}$. The number of stars per unit volume at point (r, z) contributing to the observed magnitude bin $\mathrm{d}m_i$, with $M_i = M_i - 2.5\log(r/10\mathrm{pc})^2$, is thus proportional to $r^{-2} \times \rho_g(r,z)$. The number of counts per unit of solid angle Ω (e.g. deg^2) in a magnitude bin in the direction (ℓ, b), is then proportional to

$$\int r^{-2}\,\rho_g(r,z)\,\Omega\,r^2\mathrm{d}r \propto \int \rho_g(r,z)\,\mathrm{d}r. \qquad (A.1)$$

We have therefore integrated the density models of Eqs. (4) and (5) of Wainscoat et al. (1992) for the disk and the bulge, respectively, on a typical line of sight for our fields (e.g. $l = 0$, $b = 2°$). For the disk,

$$\rho_{gD}(r,z) = \rho_{0g} \exp\left[-(R - R_0)/h - |z|/h_z\right] \qquad (A.2)$$

where ρ_{0g} is the disk density of red giants in the solar neigbourhood, R is the distance from the Galactic Center within the plane, $R_0 = 8.5$ kpc is the distance from the Sun to the Galactic Center, $h = 3.5$ kpc and $h_z = 325$ pc for the giants. For $r < R_0$, $R–R_0 = -r$; $r > R_0$, $R–R_0 = r–2R_0$; and at $b = 2°$, $z/h_z = r/(9.3\ \mathrm{kpc})$. The integrations of Eqs. (A.1), (A.2) over r along the line of sight (ℓ, b), from 0 to R_0 and from R_0 to ∞, respectively, are straightforward, yielding, in the direction $\ell = 0$, $b = 2°$, $N_F \propto 20\rho_{0g}$ for the disk counts with $r < R_0$, and $N_{Bk} \propto 12\rho_{0g}$ for the disk counts with $r > R_0$.

For the bulge,

$$\rho_{gB}(r,z) = 3.6 \times \rho_{0g}\, x^{-1.8} \exp(-x^3) \qquad (A.3)$$

where

$$x = \sqrt{R^2 + (1.6z)^2}/R_1^2 = \sqrt{R_0^2[\ell^2 + (1.6b)^2] + r'^2}/R_1^2 \qquad (A.4)$$

where $R_1 = 2.0$ kpc is the bulge "radius". However, for the small values of ℓ and b in the considered fields, most of the integral of $\rho_{gB}(r,z)$ comes from bulge points with $x \ll 1$. Therefore, the term $\exp(-x^3)$ may be neglected in Eq. (A.3). In the direction $\ell = 0$, $b = 2°$, the bulge counts are thus proportional to

$$3.6 \times \rho_{0g} \int_{-\infty}^{+\infty} x^{-1.8} \mathrm{d}r' \tag{A.5}$$

or

$$3.6 \times \rho_{0g}\, R_1 (R_0/R_1)^{-0.8} [b^2 + (\ell/1.6)^2]^{-0.4} \times \int_{-\infty}^{+\infty} (y^2+1)^{-0.9} \mathrm{d}y \tag{A.6}$$

yielding for the bulge counts, in the direction $\ell = 0$, $b = 2°$, $N_{\mathrm{Bu}} \propto 57 \rho_{0g}$.

With this model, on the line of sight $\ell = 0$, $b = 2°$, one thus expects to find about 65% of bulge sources, 22% of disk sources with $r < R_0$, and 13% of disk sources with $r > R_0$, among the ISOGAL detected sources.

Remark. Similar integrals intervene in the computation of the total stellar mass column densities $M_{\mathrm{cd}} = \int_0^{+\infty} \rho_g(r,z)\, \mathrm{d}r$, yielding, with this model:

$$M_{\mathrm{cdBu}}(M_\odot\ \mathrm{kpc}^{-2}) = 100 \times \rho_{M0}(M_\odot\ \mathrm{kpc}^{-3}) \times \left[b^2 + (\ell/1.6)^2\right]^{-0.4} \tag{A.7}$$

for the mass column density of the bulge, where b and ℓ are expressed in degrees. ρ_{M0} is the stellar mass density in the solar neighbourhood expressed in $M_\odot$ per kpc^3. We will adopt the value of Chabrier (2001) $\rho_{M0} = 4.5\ 10^7\ M_\odot\,\mathrm{kpc}^{-3}$. Since most of the bulge sources are close to the Galactic Center, one can directly infer the projected bulge mass per solid angle unit, e.g. per square degree. For instance, in the direction $\ell = 0$, $b = 2°$,

$$\Sigma_{\mathrm{Bu}(0,2)} \approx 5.7 \times 10^7\ M_\odot\,\mathrm{deg}^{-2}. \tag{A.8}$$

Acknowledgements. We thank K. S. Jeong and M. Groenewegen for providing detailed results of modelling the infrared emission of AGB stars, and A. Robin & J. Blommaert for helpful discussions.

This research is supported by the Project 1910-1 of Indo-French Center for the Promotion of Advanced Research (CEFIPRA).

The DENIS project is supported, in France by the Institut National des Sciences de l'Univers, the Education Ministry and the Centre National de la Recherche Scientifique, in Germany by the State of Baden-Würtemberg, in Spain by the DGICYT, in Italy by the Consiglio Nazionale delle Ricerche, in Austria by the Fonds zur Förderung der wissenschaftlichen Forschung und Bundesministerium für Wissenschaft und Forschung.

This publication makes use of data products from the Two Micron All Sky Survey, which is a joint project of the University of Massachusetts and the Infrared Processing and Analysis Center/California Institute of Technology, funded by the National Aeronautics and Space Administration and the National Science Foundation.

This research made use of data products from the Midcourse Space Experiment, the processing of which was funded by the Ballistic Missile Defence Organization with additional support from NASA office of Space Science.

MS is supported by the Fonds zur Förderung der wissenschaftlichen Forschung (FWF), Austria, under the project number J1971-PHY.

References

Alard, C., Blommaert, J. A. D., Césarsky, C., et al. 2001, ApJ, 552, 289
Bertelli, G., Bressan, A., Chiosi, C., et al. 1994, A&AS, 106, 275
Blommaert, J. A. D. L., Ganesh, S., Omont, A., et al. 2001, Tetons 4: Galactic Structure, Stars and the Interstellar Medium, ASP Conf. Ser., 231, 541
Chabrier, G. 2001, ApJ, 554, 1274
Césarsky, C., Abergel, A., Agnese, P., et al. 1996, A&A, 315, L32
Draine, B. T., & Lee, H. M. 1984, ApJ, 285, 89
Egan, M. P., Price, S. D., Moshir, M. M., et al. 1999, MSX Point Source Catalog Explanatory Guide (AFRL-VS-TR-1999-1522)
Epchtein, N., de. Batz, B., Copet, E., et al. 1994, Ap&SS, 217, 3
Epchtein, N., de. Batz, B., Capoani, L., et al. 1997, The Messenger, 87, 27
Felli, M., Comoretto, G., Testi, L., et al. 2000, A&A, 362, 199
Felli, M., Testi, L., Schuller, F., & Omont, A. 2002, A&A, 392, 971
Frogel, J. A., & Whitford, A. E. 1987, ApJ, 320, 199
Frogel, J. A., Tiede, G. P., & Kuchinski, L. E. 1999, AJ, 117, 2296
Glass, I. S., Whitelock, P. A., Catchpole, R. M., et al. 1995, MNRAS, 273, 383
Glass, I. S., Ganesh, S., Alard, C., et al. 1999, MNRAS, 308, 127
Glass, I. S. 1999, in Handbook of Infrared Astronomy (Cambridge University Press)
Glass, I. S., & Schultheis, M. 2002, MNRAS, 337, 519
Groenewegen, M. A. T. 1997, in The Impact of Large Scale Near-IR Sky Surveys, ed. F. Garzon, N. Epchtein, A. Omont, et al. (Kluwer), 165
Hennebelle, P., Pérault, M., Teyssier, D., et al. 2001, A&A, 365, 598
IRAS Science Team 1986, Atlas of Low Resolution Spectra, ed. F. M. Olnon, & E. Raimond, A&AS, 65, 607 (LRS)
Jeong, K. S., Winters, J. M., Le Bertre, T., & Sedlmayr, E. 2002, in Mass-losing Pulsating Stars and their Circumstellar Matter, ed. Y. Nakada, M. Honma, & M. Sekiin
Jiang, B., Omont, A., Ganesh, S., et al. 2003, A&A, 400, 903
Jura, M. 1987, ApJ, 313, 743
Le Bertre, T., & Winters, J. M. 1998, A&A, 334, 173
Le Bertre, T., Matsuura, M., Winters, J. M., et al. 2001, A&A, 376, 997
Omont, A., Ganesh, S., Alard, C., et al. 1999, A&A, 348, 755
Omont, A., Gilmore, G., Alard, C., et al. 2003, A&A, in press
Origlia, L., Ferraro, F. R., Fusi Pecci, F., & Rood, R. T. 2002, ApJ, 571, 458
Pérault, M., Omont, A., Simon, G., et al. 1996, A&A, 315, L165
Price, S. D., Egan, M. P., Carey, S. J., Mizuno, D. R., & Kuchar, T. A. 2001, AJ, 121, 2819
Schuller, F., Ganesh, S., Messineo, M., et al. 2003, A&A, in press
Schultheis, M., Ng., Y. K., Hron, J., & Kerschbaum, F. 1998, A&A, 338, 581
Schultheis, M., Ganesh, S., Simon, G., et al. 1999, A&A, 349, L69
Schultheis, M., Ganesh, S., Glass, I. S., et al. 2000, A&A, 362, 215
Schultheis, M., & Glass, I. S. 2001, MNRAS, 327, 1193
Skrutskie, M. F., Beichman, C., Capps, R., et al. 1995, A&AS, 187
van de Steene, G. C., & Jacoby, G. H. 2001, A&A, 373, 536
Wainscoat, R. J., Cohen, M., Volk, K., et al. 1992, ApJS, 83, 111
Whitelock, P. A., Menzies, J., Feast, M. W., et al. 1994, MNRAS, 267, 711